Journal of Climate

How well do global climate models simulate the variability of Atlantic tropical cyclones associated with ENSO?

--Manuscript Draft--

Manuscript Number:	
Full Title:	How well do global climate models simulate the variability of Atlantic tropical cyclones associated with ENSO?
Article Type:	Article
Corresponding Author:	Hui Wang Climate Prediction Center Camp Springs, MD UNITED STATES
Corresponding Author's Institution:	Climate Prediction Center
First Author:	Hui Wang
Order of Authors:	Hui Wang
	Lindsey Long
	Arun Kumar
	Wanqiu Wang
	Jae-Kyung E. Schemm
	Ming Zhao
	Gabriel A. Vecchi
	Timorhy E. LaRow
	Young-Kwon Lim
	Siegfried D. Schubert
	Daniel A. Shaevitz
	Suzana J. Camargo
	Naomi Henderson
	Daehyun Kim
	Jeffrey A. Jonas
	Kevin J. E. Walsh
Abstract:	The variability of Atlantic tropical cyclones (TCs) associated with El Niño-Southern Oscillation (ENSO) in model simulations is assessed and compared with observations. The model experiments are 28-yr simulations forced with the observed sea surface temperature from 1982 to 2009. The simulations were coordinated by the U.S. CLIVAR Hurricane Working Group and conducted with five global climate models (GCMs) with a total of 16 ensemble members. The model performance is evaluated based on both individual model ensemble means and multi-model ensemble mean. The latter has the highest anomaly correlation (0.86) for the interannual variability of TCs. Previous observational studies show a strong association between ENSO and Atlantic TC activity, as well as distinctions in the TC activities during eastern Pacific (EP) and central Pacific (CP) El Niño events. The analysis of track density and TC origin indicates that each model has different mean biases. Overall, the GCMs simulate the variability of Atlantic TCs well with weaker activity during EP El Niño and stronger activity during La Niña. For CP El Niño, there is a slight increase in the number of TCs as compared with EP El Niño. However, the spatial distribution of track density and TC origin is less consistent among the models. Particularly, there is no indication of increasing TC activity over the U.S. southeast coastal region as in observations. The difference between the models and observations is likely due to the bias of vertical wind shear in response to the shift of tropical heating associated with

	CP El Niño, as well as the model bias in the mean circulation.
Suggested Reviewers:	

How Well Do Global Climate Models Simulate the Variability of Atlantic Tropical Cyclones Associated with ENSO?

HUI WANG and LINDSEY LONG
NOAA/NWS/NCEP/Climate Prediction Center, College Park, Maryland and Innovim, LLC, Greenbelt, Maryland

ARUN KUMAR, WANQIU WANG, and JAE-KYUNG E. SCHEMM
NOAA/NWS/NCEP/Climate Prediction Center, College Park, Maryland

MING ZHAO and GABRIEL A. VECCHI
NOAA/Geophysical Fluid Dynamics Laboratory, Princeton, New Jersey

TIMORHY E. LAROW
Center for Ocean Atmospheric Prediction Studies, Florida State University, Tallahassee, Florida

YOUNG-KWON LIM and SIEGFRIED D. SCHUBERT
NASA Goddard Space Flight Center, Global Modeling and Assimilation Office, Greenbelt, Maryland

DANIEL A. SHAEVITZ
Department of Applied Physics and Applied Mathematics, Columbia University, New York, New York

SUZANA J. CAMARGO, NAOMI HENDERSON, and DAEHYUN KIM
Lamont-Doherty Earth Observatory, Columbia University, Palisades, New York

JEFFREY A. JONAS
Center for Climate System Research, Columbia University, New York, New York, and NASA Goddard Institute for Space Studies, New York, New York

KEVIN J. E. WALSH
School of Earth Sciences, University of Melbourne, Parkville, Victoria, Australia

Journal of Climate
Special Collection
US CLIVAR Hurricanes and Climate
Manuscript submitted 11 October 2013

Corresponding author address: Dr. Hui Wang, NOAA Climate Prediction Center, 5830 University Research Court, NCWCP, College Park, MD 20740.
E-mail: hui.wang@noaa.gov

ABSTRACT

The variability of Atlantic tropical cyclones (TCs) associated with El Niño–Southern Oscillation (ENSO) in model simulations is assessed and compared with observations. The model experiments are 28-yr simulations forced with the observed sea surface temperature from 1982 to 2009. The simulations were coordinated by the U.S. CLIVAR Hurricane Working Group and conducted with five global climate models (GCMs) with a total of 16 ensemble members. The model performance is evaluated based on both individual model ensemble means and multi-model ensemble mean. The latter has the highest anomaly correlation (0.86) for the interannual variability of TCs. Previous observational studies show a strong association between ENSO and Atlantic TC activity, as well as distinctions in the TC activities during eastern Pacific (EP) and central Pacific (CP) El Niño events. The analysis of track density and TC origin indicates that each model has different mean biases. Overall, the GCMs simulate the variability of Atlantic TCs well with weaker activity during EP El Niño and stronger activity during La Niña. For CP El Niño, there is a slight increase in the number of TCs as compared with EP El Niño. However, the spatial distribution of track density and TC origin is less consistent among the models. Particularly, there is no indication of increasing TC activity over the U.S. southeast coastal region as in observations. The difference between the models and observations is likely due to the bias of vertical wind shear in response to the shift of tropical heating associated with CP El Niño, as well as the model bias in the mean circulation.

1. Introduction

It is well known that El Niño–Southern Oscillation (ENSO) strongly influences the interannual variability of Atlantic tropical cyclones (TCs). El Niño (La Niña) tends to suppress (enhance) Atlantic seasonal TC activity (e.g., Gray 1984; Pielke and Landsea 1999; Bell and Chelliah 2006). Although other climate modes, such as the Atlantic Meridional Mode, the North Atlantic Oscillation, and the Madden Julian Oscillation, also modulate North Atlantic tropical cyclone activity (e.g. Kossin et al. 2010), here our focus will be placed on ENSO. The state of ENSO is one of the key climate factors considered by the National Oceanic and Atmospheric Administration (NOAA) for their Atlantic hurricane season outlooks (NOAA 2013).

Using observational data, Kim et al. (2009) found distinct differences in Atlantic TC activity associated with eastern Pacific (EP) El Niño and central Pacific (CP) El Niño. EP El Niño is the conventional El Niño with the warmest sea surface temperature (SST) anomalies in the tropical eastern Pacific, whereas CP El Niño or El Nino Modoki (Ashok et al. 2007) is a non-conventional El Niño with the warmest SST anomalies in the tropical central Pacific. The zonal shift of the warm SST anomalies indicates a change in tropical heating and consequent changes in atmospheric response.

A composite analysis of TC track density anomaly in Kim et al. (2009, their Fig. 2) displays coherent weakening in TC activity over the Caribbean Sea, Gulf of Mexico, and U.S. Atlantic east coast region during EP El Niño and strengthened TC activity over the same regions during La Niña. Surprisingly, the composite for CP El Niño is also opposite to that for EP El Niño over these regions and closely resembles the La Niña composite. The results suggest a higher chance of landfalling TCs along the Gulf coast and U.S. east coast during CP El Niño than during EP El Niño.

90 It is well recognized that global climate models (GCMs), even at a low resolution, are
91 able to simulate the interannual response of North Atlantic TCs to ENSO (e.g. Camargo et al.
92 2005, Zhao et al. 2009). However, given the distinctions in the Atlantic TC activity associated
93 with different El Niño types revealed in observations (Kim et al. 2009), it is interesting to know
94 whether state-of-the-art GCMs can reproduce the different response to the two types of El Niño.
95 Such a model capability in distinguishing the responses of Atlantic TCs to different ENSO
96 patterns is also important to both dynamical (e.g., Schemm and Long 2009) and statistical–
97 dynamical (e.g., Wang et al. 2009; Vecchi et al. 2011) hurricane seasonal prediction systems.
98 With a primary focus on climate modeling studies of TCs, the U.S. Climate Variability
99 and Predictability Research Program (CLIVAR) launched a Hurricane Working Group (HWG)
100 in 2011 (U.S. CLIVAR 2011). To improve understanding of the interannual variability and
101 trends in TC activity, as well as projections of future TC activity under a warming climate, the
102 HWG initiated a series of simulations with high-resolution atmospheric GCMs (Walsh et al.
103 2013). One set of simulations is the interannual experiment which is an Atmospheric Model
104 Intercomparison Project (AMIP) type of simulations with multiple GCMs and forced with the
105 same observed time-varying SST from 1982 to 2009. This set of simulations provides necessary
106 data to characterize TC response to ENSO in climate models.
107 This study aims to evaluate the performance of high-resolution GCMs in simulating the
108 interannual variability of Atlantic TCs associated with ENSO. The assessment is based on the
109 analysis of AMIP-type simulations with five GCMs and comparisons with observations. The
110 analysis is in collaboration with HWG members to target one of the HWG objectives involving
111 improved understanding of interannual variability of TC activity. The following three scientific
112 questions are to be addressed in this study. How is the overall performance of GCMs in

113 simulating the variability of Atlantic TCs? What are the characteristics of Atlantic TCs
114 associated with ENSO in the models? What are the possible explanations for the differences
115 between the models and observations? The study is expected to provide some insights into the
116 basic characteristics of Atlantic TC activity associated with different types of ENSO in GCMs.

117 This paper is organized as follows. Section 2 provides a brief description of data,
118 models, and analysis methods used. Section 3 characterizes the Atlantic TC activity associated
119 with ENSO in observations. The performance of GCMs in simulating the variability of the
120 Atlantic TCs is assessed in section 4. Some possible explanations for the differences between
121 the model simulations and observations are explored in section 5. Conclusions are given in
122 section 6.

123

124 **2. Data and models**

125 The data used in this study consist of SST, Atlantic TC tracks, precipitation, 200-hPa and
126 850-hPa zonal winds over a 28-yr (1982–2009) period from both observations and simulations
127 with five atmospheric GCMs. For observations, the SST data are taken from the Hadley Centre
128 Sea Ice and Sea Surface Temperature (HadISST) data set (Rayner et al. 2003) on a $1^{o} \times 1^{o}$
129 (latitude × longitude) grid. The 28-yr monthly mean SSTs were also prescribed as low boundary
130 forcing for the GCMs. The Atlantic TC track data are from the National Hurricane Center
131 Atlantic Hurricane Best Track Data (HURDAT2; Landsea et al. 2004). The precipitation data
132 are from the Climate Prediction Center (CPC) Merged Analysis of Precipitation (CMAP) data set
133 (Xie and Arkin 1997). The 200-hPa and 800-hPa zonal winds used to derive vertical wind shear
134 are from the National Centers for Environmental Prediction – Department of Energy (NCEP –
135 DOE) reanalysis 2 (R2; Kanamitsu et al. 2002). Both precipitation and zonal winds are monthly
136 mean data on a $2.5^{o} \times 2.5^{o}$ grid.

137 The five GCMs employed for the HWG interannual experiments (1982–2009) are the
138 Florida State University (FSU) model (Cocke and LaRow 2000), Geophysical Fluid Dynamics
139 Laboratory (GFDL) model (Zhao et al. 2009), National Aeronautics and Space Administration
140 (NASA) Goddard Institute for Space Studies (GISS) model E2 (Schmidt et al. 2013), NASA
141 Goddard Space Flight Center (GSFC) GEOS-5 model (Rienecker et al. 2008; Molod et al. 2012),
142 and NCEP Global Forecast System (GFS) model (Saha et al. 2013). Table 1 lists the number of
143 ensemble runs, model data resolutions, which are close to model resolutions, and TC tracking
144 algorithms for the five models. The ensemble members vary from two to five with a total of 16
145 runs. Horizontal resolutions range from about 0.5^{o} to 1^{o}. TC track data were provided by each
146 modeling group with different tracking algorithms. More detailed descriptions of the models can
147 be found in Walsh et al. (2013).

148 The Atlantic TC activity is quantified by the annual total number of TCs, as well as the
149 spatial distribution of track density and TC origin. Given the spatially discrete nature of TC
150 tracks, the track density is derived as follows: (a) the number of TCs passing through each $5^{o} \times$
151 5^{o} box analyzed on a $1^{o} \times 1^{o}$ grid resolution during an entire hurricane season is first counted;
152 and (b) the TC counts are then averaged with the TC numbers in the $5^{o} \times 5^{o}$ boxes for eight
153 surrounding grid points with a weighting coefficient of 0.5 for the center grid point and 1/16 for
154 each surrounding grid point. This is done in the same way as Kim et al. (2009) to ensure a
155 spatially smoothed distribution. Composites of SST, precipitation, and vertical wind shear
156 anomalies averaged over August–October (ASO), the peak of the Atlantic hurricane season, are
157 examined for different ENSO categories. The statistical significance of the composite anomalies
158 is estimated by the Monte Carlo technique (e.g., Wilks 1995). The analysis is performed for both
159 observations and multi-model ensemble (MME) mean, as well as individual model ensemble

means. The MME mean is obtained by averaging individual model ensemble means. In this way, each model is treated with an equal weight for the MME, regardless of the number of ensemble members.

3. Variability of Atlantic TCs associated with ENSO in observations

During the 28-yr period (1982–2009), there were five EP El Niño (1982, 1986, 1991, 1997, and 2006) and five CP El Niño (1987, 1994, 2002, 2004, and 2009) years identified based on the definition of McPhaden et al. (2011), and eight La Niña years (1983, 1984, 1988, 1995, 1998, 1999, 2005, 2007). Figure 1 shows the composite of ASO seasonal mean SST anomalies for EP El Niño, CP El Niño, and La Niña, respectively. Compared to EP El Niño (Fig. 1a), the SST anomalies in CP El Niño (Fig. 1b) shift towards the west. This may lead to significant changes in tropical heating for the atmosphere between the two types of El Niño. The amplitude of the CP El Niño SST anomalies (~ 1 K) is smaller than the EP El Niño (~ 1.5 K), but comparable to the La Niña (~ 1 K, Fig. 1c).

Similar composites are shown in Fig. 2 for TC track density (top row) and track density anomaly (middle row), respectively, associated with the three ENSO types. In La Niña years (Fig. 2c), track density displays high values (> 1) across the North Atlantic basin. Areas with track densities greater than 1.5 are found in the central main development region (MDR; 10^{o} – 20^{o}N, 20^{o} – 80^{o}W), the Gulf of Mexico, and U.S. east coastal region. In contrast, track density is relatively low over these regions for EP El Niño (Fig. 2a), but increases considerably for CP El Niño (Fig. 2b), particularly in the MDR and U.S. southeast coastal region.

Consistent with the track density patterns, track density anomalies are generally below normal across the basin for EP El Niño (Fig. 2d), with the largest negative anomalies over the Gulf and MDR, and above normal during La Niña (Fig. 2f). Associated with CP El Niño (Fig.

184 2e), positive track density anomalies are found over the MDR, the Caribbean Sea, Gulf coast and
185 the southeast coast, and negative anomalies further to the east, as well as in the west Gulf of
186 Mexico. The results indicate that relative to EP El Niño, there is a high chance of landfalling
187 TCs along the U.S. southeast coast during CP El Niño.

188 The spatial distributions of total TC origins for the three ENSO categories are also shown
189 in Fig. 2 (bottom row). For a fair comparison with five EP El Niño and five CP El Niño, TC
190 origins for La Niña are also shown for five episodes that occurred in the most recent years.
191 There are increased TC origins over the MDR during CP El Niño (Fig. 2h) as compared to EP El
192 Niño (Fig. 2g) and an additional increase of TC formation over the Gulf of Mexico during La
193 Niña (Fig. 2i).

194 Although the sample size for ENSO composites is very limited over the 28 years, the
195 composite anomalies in Fig. 2 (middle row) are statistically significant above the 90% level. The
196 anomaly patterns also resemble those in Kim et al. (2009) with longer records (57 yrs, 1950–
197 2006). Additionally, the sampling issue can be partially addressed by using HWG interannual
198 experiments which provide more atmospheric realizations than for the observations. Although
199 the AMIP type of simulations does not increase the sample size of ENSO events, the ensemble of
200 AMIP runs presented in the next section increases the sample size of atmospheric realizations for
201 a fixed set of ENSO events. This can effectively enhance the signal-to-noise ratio (Kumar and
202 Hoerling 1995) and thereby provide a more reliable estimate for the ENSO-forced variability of
203 the Atlantic TCs.
204
205 **4. Variability of Atlantic TCs associated with ENSO in GCMs**

206 The climatology and interannual variability of the annual number of Atlantic TCs are
207 examined first. Figure 3 shows the time series of the annual number of Atlantic TCs from 1982

208 to 2009 for both observations and model simulations, including MME mean and individual
209 model ensemble means. Both observations and MME display an upward trend over the 28-yr
210 period. The grey shading in Fig. 3 denotes the range of ± one standard deviation of the spreads
211 of the five individual model ensemble means around the MME mean. Over 80% (23 out of 28
212 yrs) of the observations fall into this range. Obviously, the GFS model has very high numbers of
213 TCs and the GISS model has low numbers of TCs.

214 Table 2 summarizes the TC statistics for the observations and model simulations,
215 including the climatological mean value, variance of interannual variability, linear trend over the
216 28 years, anomaly correlation (AC) between the models and observations, and root-mean square
217 error (RMSE). The GFDL model (12.7) and GSFC model (10.9) have a mean value close to the
218 observations (11.7). In contrast, the climatology in the GISS model (6.2) is only about a half of
219 the observations while the GFS model (22.0) has double the number in observations. The
220 strength of the interannual variability in the GSFC and GFS models is comparable to
221 observations and weaker in the other models and the MME. The linear trends in all models (~ 2
222 TCs per decade) are weaker than in the observations (~ 4 TCs per decade). AC is highest for the
223 MME (0.86), followed by the GFDL (0.74) and GFS (0.73) models. This implies that 74% of
224 the observed interannual TC variance is captured by the time series of the MME mean number of
225 TCs and 54% is captured by the GFDL and GFS models. Additionally, the MME has the
226 smallest RMSE. Due to the large mean biases, the GFS and GISS models have relatively large
227 RMSEs. In terms of the five parameters in Table 2 (i.e., mean, interannual variability, trend, AC,
228 and RMSE), the overall performance of the MME, GFDL and GSFC models is better than that of
229 the FSU, GISS, and GFS models. It should be noted that both the GFDL and GSFC models have

230 a higher resolution than the other three models. This may suggest that a GCM with a higher
231 resolution gets better performance in simulating the interannual variability of Atlantic TCs.

232 The average number of TCs for each ENSO category is examined in Table 3 and
233 compared with the corresponding 28-yr climatology for both observations and simulations. In
234 the observations, there are about 7, 10, and 15 TCs each hurricane season in EP El Niño, CP El
235 Niño, and La Niña, respectively, equivalent to 58%, 87%, and 125% of the mean value (11.7).
236 All models show consistent increases in the number of TCs from EP El Niño to CP El Niño and
237 further increases to La Niña, except for the GSFC model. However, the changes in TC counts
238 from one ENSO type to another in the models are much more conservative than in the
239 observations. In the MME, for instance, there is a 15% increase in TCs from EP El Niño to CP
240 El Niño and an additional 16% increase to La Niña in terms of the mean value. The
241 corresponding changes in observations are 29% and 38%. The results indicate a weaker
242 interannual variability of Atlantic TCs in the model simulations. It should also be noted that the
243 MME mean approach may reduce the variability of TC counts in the models.

244 The spatial characteristics of mean TC activity are presented in Fig. 4 for both
245 observations and simulations in the form of 28-yr mean track densities and total TC origins
246 during the entire 28 years. Compared to the observations (Fig. 4a), each model has different
247 mean biases. Among the five models, the GFDL model (Fig. 4d) is closest to the observations
248 for both the magnitude and spatial coverage of track density. The FSU, GSFC, and GFS models
249 (Figs. 4c, 4f, 4g) have a very high track density (> 3) over the west MDR, east–central MDR,
250 and most of the North Atlantic basin, respectively, whereas the GISS model (Fig. 4e) has a very
251 low track density over the basin. The MME mean pattern (Fig. 4h) shows a higher track density

252 in the MDR than the observations (Fig. 4a) and a lower track density over the U.S. east coastal
253 regions. Overall, the MME is better than most individual models.

254 The TC origins in observations (Fig. 4b) are characterized by two regions with large
255 populations, one over the MDR and the other over the Gulf of Mexico and adjacent sectors of the
256 Atlantic Ocean and Caribbean Sea. The FSU, GSFC, and GFS models exhibit very dense TC
257 origins over the central and to the south of the MDR (Fig. 4i), to the south of the east MDR (Fig.
258 4l), and to the south and east of the MDR (Fig. 4m), respectively. The GISS model shows a lack
259 of TC formations over the east MDR. The GFDL model (Fig. 4j) and MME (Fig. 4n) have a
260 distribution of TC origins closer to the observations than the other models. The model biases in
261 the distribution of TC origins are consistent with the biases of track density and mean number of
262 TCs. For example, the dense TC origins in the FSU and GSFC models (Figs. 4i and 4l) lead to
263 high track density over the regions to the northwest of the TC origins (Figs. 4c and 4f). If the
264 unrealistic TC origins to the east of the MDR in the GFS model (Fig. 4m) are removed, the mean
265 number of TCs is significantly reduced from 22.0 to 11.7, matching the observed value, and
266 leading to a track density distribution much closer to the observations (not shown).

267 Similar to the ENSO composites of track density for observations (Fig. 2, top row), Fig. 5
268 displays the ENSO composites of track density for individual model ensemble means, as well as
269 MME mean. In spite of the distinct biases in each model revealed in Fig. 4, the composites
270 consistently show relatively low track densities during EP El Niño (left column) in all models
271 and high track densities during La Niña in most models (right column), except for the GSFC
272 model. Furthermore, there is a clear increase in track density from EP El Niño to CP El Niño
273 (Fig. 5, middle column).

The corresponding composites for track density anomaly are illustrated in Fig. 6. The track density anomalies in the GCMs are generally below normal across the basin during EP El Niño (left column) and above normal during La Niña (right column). In some spots, the negative anomalies associated with EP El Niño (left column) become positive during CP El Niño (middle column). The results in Figs. 5 and 6 suggest that the GCMs are able to capture some of the observed features of the Atlantic TC activity associated with ENSO. Qualitatively, there is less TC activity associated with EP El Niño, more activity associated with La Niña, and increasing TC activity during CP El Niño with respect to EP El Niño. However, the patterns of track density vary from model to model and differ from observations. Particularly, there are no indications of increasing landfalling TCs along the U.S. southeast coast during CP El Niño in the model simulations.

The modeled TC origins over five years from one ensemble member of each model are shown in Fig. 7 for each ENSO category. Relative to EP El Niño (left column), there are increases in the formation of TCs over or near the MDR during CP El Niño (middle column) and La Niña (right column) in some models, such as the GSFC and GFS models. Only the GFDL model shows some increase in TC origins at high latitudes between 20^{o}N and 40^{o}N, especially during CP El Niño. Unlike observations (Fig. 2i), there are no increases in TC origins over the Gulf of Mexico and west Caribbean Sea in all models during La Niña. This may be related to the model bias in simulating the TC formations over these regions (Fig. 4). The differences in TC origins among the three ENSO categories in the MME (Fig. 7, bottom row) are not as large as in the observations (Fig. 2, bottom row). This is another indication of relatively weak interannual variability of Atlantic TCs in GCMs.

297 **5. Possible explanations for model biases**

298 The changes in both the mean and variability of Atlantic TCs is accompanied by changes
299 in atmospheric circulation (e.g., Goldenberg and Shapiro 1996; Goldenberg et al. 2001).
300 Therefore, in order to understand the mean biases of TC activity in GCMs, Fig. 8 shows the ASO
301 season climatology of vertical shear of zonal wind between 200 and 850 hPa derived from
302 observations and mean biases for individual model ensemble means and the MME mean. The
303 regions of weak mean vertical wind shear (< 10 m s^{-1}, Fig. 8a) coincide with the regions of high
304 mean track density and TC origins in observations (Figs. 4a and 4b).

305 The mean bias in the vertical wind shear may account for the mean bias in Atlantic TC
306 activity in some models. In the FSU model (Fig. 8b), for instance, a large negative bias of
307 vertical wind shear (over –10 m s^{-1}) in the west MDR leads to a close-to-zero mean state of
308 vertical wind shear, which favors the generation and development of TCs. This is consistent
309 with the mean bias of high track density and TC origins over this region (Figs. 4c and 4i). In the
310 GISS model (Fig. 8d), a positive bias of vertical wind shear in the east MDR enhances the mean
311 vertical wind shear and prevents TCs from occurring over this area. As a result, TC tracks and
312 TC origins shift towards the west (Figs. 4e and 4k).

313 Both individual model ensemble means (Figs. 8b–8f) and the MME mean (Fig. 8g)
314 exhibit negative biases in vertical wind shear over and/or near the MDR and positive biases to
315 the north, especially over the Gulf coast and U.S. southeast coast. Consequently, there are biases
316 of high track density and dense TC origins at low latitudes and low track density and sparse TC
317 origins over the Gulf and U.S. southeast coast in the models (Fig. 4).

318 Figure 9 displays the composites of ASO season vertical wind shear anomalies associated
319 with the three ENSO categories for observations (top row) and MME (bottom row), respectively.

Overall, the model circulation response to different ENSO SST anomalies agree with the observations, both with positive vertical wind shear anomalies to the south of 20°N associated with EP El Niño (left column) and negative anomalies associated with La Niña (right column). The circulation response to CP El Niño is less significant or spatially coherent over the subtropical North Atlantic (middle column). This is likely due to the weak amplitude and small area-coverage of the CP El Niño SST anomalies (Fig. 1). Thus the atmospheric response may be weak (e.g., Wang et al. 2013). In spite of that, it is still evident that wind shear anomalies over the MDR are largely reduced as compared to EP El Niño, a condition that is more favorable for TC activity during CP El Niño. The results present in Fig. 9 are also consistent with the better simulations of Atlantic TC activity in GCMs for EP El Niño and La Niña than for CP El Niño.

ENSO influences the Atlantic TC activity by altering vertical wind shear over the MDR through atmospheric teleconnection (e.g., Goldenberg and Shapiro, 1996). It may also change tropical Atlantic SST via local air-sea interaction (Enfield and Mayer 1997), which in turn affects the TC activity (Goldenberg et al. 2001). The composites of SST anomalies in Fig. 1 suggest very weak Atlantic SST anomalies associated with ENSO in ASO. Furthermore, diagnostics of the ENSO modulation of TC activity using a genesis potential index identified vertical wind shear as one of the main environmental factors responsible for this modulation in the North Atlantic (Camargo et al. 2007). Therefore, the atmospheric response to tropical heating related to ENSO SST anomalies and atmospheric teleconnection are likely the primary processes responsible for the ENSO impact.

The westward shift of warm SST anomalies from EP El Niño to CP El Niño (Fig. 1) may lead to changes in tropical heating. In the tropics, precipitation associated with deep convection is a good indicator of tropical heating in the atmosphere. Similar to Wang et al. (2012), the

343 composites of ASO season precipitation anomalies over the tropical Pacific are used to illustrate
344 and verify the changes in tropical heating, as shown in Fig. 10. In both observations and the
345 MME mean of the GCM simulations, associated with EP El Niño (Figs. 10a and 10d), there are
346 positive precipitation anomalies across the central and eastern equatorial Pacific. Associated
347 with CP El Niño (Figs. 10b and 10e), precipitation anomalies shift towards the west with no
348 large anomalies over the eastern Pacific. In La Niña, negative precipitation anomalies cross the
349 tropical Pacific (Figs. 10c and 10f). In general, the GCMs reproduce the observed major features
350 of precipitation anomalies over the tropical Pacific for different types of ENSO. On the other
351 hand, precipitation response to ENSO over the tropical North Atlantic (not shown) varies
352 considerably across the models, which may contribute to the model diversity in simulating the
353 TC variability associated with ENSO.

354 There are also differences in precipitation between observations and simulations over the
355 tropical Pacific, such as weaker precipitation anomalies in the models between 160°E and the
356 dateline for all ENSO categories. These differences may be related to model convection
357 schemes and model sensitivity to SST. Together with model biases in mean circulation (not
358 shown), they may modify the Rossby-wave source (Sardeshmukh and Hoskins 1998) and thus
359 affect the detailed structure of circulation response to ENSO.

360 Figure 11 gives a simple example of changes in vertical wind shear associated with a
361 westward shift of warm SST anomalies from the Niño-3 region (5°S – 5°N, 90° – 150°W) to the
362 Niño-4 region (5°S – 5°N, 150°W – 160°E). First, the ASO season vertical wind shear anomalies
363 are regressed against the Niño-4 and Niño-3 SST indices, separately. The differences between
364 the two sets of regression coefficients are shown for observations (left panel) and the MME
365 (right panel), respectively. Both the observations and the MME exhibit a similar large-scale

366 wave train pattern originating from the western and central equatorial Pacific and along a great
367 circle route to tropical Atlantic. A close inspection of Fig. 11 reveals some differences in the
368 changes of vertical wind shear over the tropical North Atlantic between the observations and
369 simulations. Negative wind shear anomalies are found to the north of the MDR in the
370 observations (Fig. 11a) whereas positive anomalies are found over the MDR in the MME (Fig.
371 11b). The results illustrate the difference between the observations and GCMs in North Atlantic
372 vertical wind shear response to the shift of tropical Pacific SST anomalies. The difference may
373 cause further changes in the responses of Atlantic TCs to the shift of SST anomalies.
374
375 **6. Summary and conclusions**
376 Based on the analysis of the HWG interannual experiments, the GCM's performance in
377 simulating the variability of Atlantic TCs associated with ENSO are assessed. The results
378 indicate that each model has different mean biases in terms of track density and TC origin.
379 Among the five models, the GFDL model with a relatively high resolution has the best
380 performance. The MME mean has the highest anomaly correlation for the number of TCs and
381 the least RMSE. Therefore, using an MME should be considered a better approach for
382 dynamical hurricane season prediction than using a single model. Overall, the GCMs simulate
383 the variability of Atlantic TCs well with weaker activities during EP El Niño and stronger
384 activities during La Niña. For CP El Niño, there is a slight increase in the number of TCs as
385 compared with EP El Niño. However, the spatial distribution of track density and TC origin is
386 less consistent among the models. Particularly, there is no indication of increasing TC activity
387 over the U.S. southeast coastal region as found in observations. The differences between the
388 models and the observations may be due to the bias of vertical wind shear in response to the shift
389 of tropical heating associated with CP El Niño, as well as the model bias in the mean circulation.

390 It should also be noted that there are limited sample sizes for both EP and CP El Niño events in
391 the observations. The differences between EP and CP El Niño composites may not be just due to
392 ENSO response, but also contain some random component.

393 There are at least two factors that may affect the results presented in this paper. One is
394 the model sensitivity to different SST data sets (e.g., LaRow 2013). For example, the FSU
395 model forced with the NOAA optimum interpolation SST version 2 (OISST v2; Reynolds et al.
396 2002) may improve the simulations of Atlantic TC activity with a better TC climatology (11.5)
397 and RMSE (4.5) than those forced with HadISST (Table 2). Knowledge of the model sensitivity
398 to SST forcing may help estimate the uncertainty of the model simulated TCs. In this study,
399 different TC tracking algorithms were employed by the five modeling groups for their GCMs
400 (Table 1). Track density and TC origin in the models may also be sensitive to the algorithms
401 used (e.g., Horn et al. 2013). A unified tracking algorithm may be helpful to reduce the related
402 uncertainty for model assessment.

403 The impact of ENSO on Atlantic TC activity may have some implications for projections
404 of future TC variability under a warming climate. Studies have shown an increase in tropical
405 Atlantic wind shear (Vecchi and Soden, 2007) and a reduction of Atlantic TCs associated with
406 global warming with a high-resolution GCM (Zhao and Held 2010). In more recent studies, no
407 robust changes in North Atlantic TC activity were found in the 21st century simulations with
408 low-resolution models (Camargo 2013; Tory et al. 2013). On the other hand, downscaling
409 studies of these simulations lead to contradictory results, varying from a significant decrease
410 (Knutson et al. 2013), ambiguous trends (Villarini and Vecchi 2013), to a significant increase
411 (Emanuel 2013) in North Atlantic TC activity by the end of the 21st century. In addition to
412 possible changes in the mean TC activity, the variability of TC activity is also expected to

change as the intensity of CP El Niño (EP El Niño) would increase (decrease) under a warming climate (Kim and Yu 2012). In fact, CP El Niño has been documented to occur more frequently in the most recent two decades (Yeh et al. 2009), which could be a manifestation of global warming in observations.

There is a possibility that the relationship between Atlantic TC activity and ENSO under the present-day climate found in Kim et al. (2009) might not be maintained under a warming climate. Indeed, changes in atmospheric teleconnection in response to ENSO have been detected in model simulations for the 21st century (e.g., Stevenson 2012). This would add additional uncertainty to the future projection of Atlantic TC variability. Nevertheless, this study indicates the feasibility of utilizing high-resolution GCMs to assess the Atlantic TC activity associated with ENSO for climate change projections.

Acknowledgments. This work was carried out as part of a Hurricane Working Group (HWG) activity supported by the U.S. CLIVAR. The authors thank the Lamont-Doherty Earth Observatory of Columbia University for archiving model data and making them accessible online. The authors also thank Prof. Kerry A. Emanuel for providing useful comments and suggestions during a U.S. CLIVAR HWG review of the paper.

References

Ashok, K., S. K. Behera, S. A. Rao, H. Weng, and T. Yamagata, 2007: El Niño Modoki and its possible teleconnection. *J. Geophys. Res.*, **112,** C11007, doi:10.1029/2006JC003798.

Bell, G. D., and M. Chelliah, 2006: Leading tropical modes associated with interannual and multidecadal fluctuations in North Atlantic hurricane activity. *J. Climate*, **19,** 590–612.

Camargo, S. J., 2013: Global and regional aspects of tropical cyclone activity in the CMIP5 models. J. Climate, doi:10.1175/JCLI-D-12-00549.1, in press.

Camargo, S. J., A. G. Barnston, and S. E. Zebiak, 2005: A statistical assessment of tropical cyclone activity in atmospheric general circulation models. *Tellus*, **57A,** 589–604.

Camargo, S. J., K. A. Emanuel, and A. H. Sobel, 2007: Use of a genesis potential index to diagnose ENSO effects on tropical cyclone genesis. *J. Climate*, **20**, 4819-4834.

Camargo, S. J., and S. E. Zebiak, 2002: Improving the detection and tracking of tropical cyclones in atmospheric general circulation models. *Wea. Forecasting*, **17,** 1152–1162.

Cocke, S. D., and T. E. LaRow, 2000: Seasonal predictions using a regional spectral model embedded within a coupled ocean–atmospheric model. *Mon. Wea. Rev.*, **128,** 689–708.

Emanuel, K. A., 2013: Downscaling CMIP5 climate models shows increased tropical cyclone activity over the 21st century. *Proc. Nat. Acad. Sci.*, **110**, doi:10.1073/pnas.1301293110.

Enfield, D. B., and D. A. Mayer, 1997: Tropical Atlantic SST variability and its relation to El Niño – Southern Oscillation. *J. Geophys. Res.*, **102,** 929–945.

Goldenberg, S. B., and L. J. Shapiro, 1996: Physical mechanisms for the association of El Niño and West African rainfall with Atlantic major hurricane activity. *J. Climate*, **9,** 1169–1187.

Goldenberg, S. B., C.W. Landsea, A. M. Mestas-Nuñez, and W. M. Gray, 2001: The recent increase in Atlantic hurricane activity: Cause and implications. *Science*, **293,** 474–479.

456 Gray, W. M., 1984: Atlantic seasonal hurricane frequency. Part I. El Niño and 30 mb quasi-
457 biennial oscillation influences. *Mon. Wea. Rev.*, **112,** 1649–1668.
458 Horn, M., K. J. E. Walsh, and A. Ballinger, 2013: A phenomenon-based tracking scheme for
459 high-resolution climate models. U.S. CLIVAR Hurricane Workshop, June 5–7, 2013,
460 Princeton, New Jersey.
461 Kanamitsu, M., W. Ebisuzaki, J. Woollen, S.-K. Yang, J. J. Hnilo, M. Fiorino, and G. L. Potter,
462 2002: NCEP–DOE AMIP-II Reanalysis (R-2). *Bull. Amer. Meteor. Soc.*, **83,** 1631–1643.
463 Kim, H.-M., P. J. Webster, and J. A. Curry, 2009: Impact of shifting patterns of Pacific Ocean
464 warming on North Atlantic tropical cyclones. *Science*, **325,** 77–80.
465 Kim, S. T., and J.-Y. Yu, 2012: The two types of ENSO in CMIP5 models. *Geophys. Res. Lett.*,
466 **39,** L11704, doi:10.1029/2012GL052006.
467 Knutson, T. R., J. J. Sirutis, G. A. Vecchi, S. Garner, M. Zhao, H.-S. Kim, M. Bender, R.E.
468 Tuleya, I.M. Held, and G. Villarini, 2013: Dynamical downscaling projections of twenty-
469 first-century Atlantic hurricane activity: CMIP3 and CMIP5 model-based scenarios. *J.*
470 *Climate*, **26**, 6591–6617.
471 Kossin, J. P., S. J. Camargo, and M. Sitkowski, 2010. Climate modulation of North Atlantic
472 hurricane tracks. *J. Climate*, **23**, 3057–3076.
473 Kumar, A., and M. P. Hoerling, 1995: Prospects and limitations of atmospheric GCM climate
474 predictions. *Bull. Amer. Meteor. Soc.*, **76,** 335–345.
475 Landsea, C. W., 2000: El Niño/Southern Oscillation and the seasonal predictability of tropical
476 cyclones. *El Niño and the Southern Oscillation: Multiscale Variability and Global and*
477 *Regional Impacts*. Cambridge University Press, 149–182.
478 Landsea, C. W., C. Anderson, N. Charles, G. Clark, J. Dunion, J. Fernandez-Partagas, P.
479 Hungerford, C. Neumann, and M. Zimmer, 2004: The Atlantic hurricane database re-
480 analysis project: Documentation for the 1851–1910 alterations and additions to the

481 HURDAT database. *Hurricanes and Typhoons: Past, Present and Future*, R. J.
482 Murname and K.-B. Liu, Eds., Columbia University Press, 177–221.
483 LaRow, T. E., 2013: The impact of SST bias correction on North Atlantic hurricane retrospective
484 forecasts. *Mon. Wea. Rev.*, **141,** 490–498.
485 LaRow, T. E., Y.-K. Lim, D. W. Shin, E. P. Chassignet, and S. Cocke, 2008: Atlantic basin
486 seasonal hurricane simulations. *J. Climate*, **21,** 3191–3206.
487 McPhaden, M.J., T. Lee, and D. McClurg, 2011: El Niño and its relationship to changing
488 background conditions in the tropical Pacific Ocean. *Geophys. Res. Lett*., **38**, L15709,
489 doi:10.1029/2011GL048275.
490 Molod, A., L. Takacs, M. Suarez, J. Bacmeister, I.-S. Song, and A. Eichmann, 2012: The GEOS-
491 5 Atmospheric General Circulation Model: Mean Climate and Development from
492 MERRA to Fortuna. *NASA Technical Report Series on Global Modeling and Data*
493 *Assimilation*, NASA/TM-2012-104606, **28,** 117 pp.
494 NOAA, cited 2013: Atlantic hurricane outlook and summary archive. [Available online at http://
495 www.cpc.ncep.noaa.gov/products/outlooks/hurricane-archive.shtml.]
496 Pielke, R. A., Jr., and C. W. Landsea, 1999: La Nina, El Nino, and Atlantic hurricane damages in
497 the United States. *Bull. Amer. Meteor. Soc.*, 80, 2027–2033.
498 Rayner, N. A., D. E. Parker, E. B. Horton, C. K. Folland, L. V. Alexander, D. P. Rowell, E. C.
499 Kent, and A. Kaplan, 2003: Global analyses of sea surface temperature, sea ice, and night
500 marine air temperature since the late nineteenth century. *J. Geophys. Res.*, **108**(D14),
501 4407, doi:10.1029/2002JD002670.
502 Reynolds, R. W., N. A. Rayner, T. M. Smith, D. C. Stokes, and W. Wang, 2002: An improved in
503 situ and satellite SST analysis for climate. *J. Climate*, **15,** 1609–1625.

504 Rienecker, M. M., and Coauthors, 2008: The GEOS-5 Data Assimilation System –
505 Documentation of Versions 5.0.1 and 5.1.0, and 5.2.0. *NASA Technical Report Series on*
506 *Global Modeling and Data Assimilation*, NASA/TM-2008-104606, **27,** 92 pp.
507 Saha, S. and Coauthors, 2013: The NCEP Climate Forecast System Version 2. *J. Climate*,
508 doi:10.1175/JCLI-D-12-00823.1, in press.
509 Sardeshmukh, P. D., and B. J. Hoskins, 1998: The generation of global rotational flow by steady
510 idealized tropical divergence. *J. Atmos. Sci.*, **45,** 1228–1251.
511 Schemm, J.-K. E., and L. Long, 2009: Dynamic hurricane season prediction experiment with the
512 NCEP CFS CGCM. *NOAA CTB Joint Seminar Series Extended Summaries Collection*, **3,**
513 27–29.
514 Schmidt, G. A., and Coauthors, 2013: Configuration and assessment of GISS Model E2
515 contributions to the CMIP5 archive. *J. Climate*, submitted.
516 Stevenson, S. L., 2012: Significant changes to ENSO strength and impacts in the twenty-first
517 century: Results from CMIP5. *Geophys. Res. Lett.*, **39,** L17703, doi:10.1029/2012GL
518 052759.
519 Tory, K., S. S. Chand, J. L. McBride, H. Ye, and R.A. Dare, 2013: Projected changes in late 21st
520 century tropical cyclone frequency in thirteen coupled climate models from the Coupled
521 Model Intercomparison Project Phase 5. *J. Climate*, doi:10.1175/JCLI-D-13-00010.1, in
522 press.
523 U.S. CLIVAR, 2011: U.S. CLIVAR launches two new working groups. *Variations*, **9**(1), 11.
524 Vecchi, G. A., and B. J. Soden, 2007: Increased tropical Atlantic wind shear in model projections
525 of global warming. *Geophys. Res. Lett.*, **34,** L08702, doi:10.1029/2006GL028905.
526 Vecchi, G. A., M. Zhao, H. Wang, G. Villarini, A. Rosati, A. Kumar, I. M. Held, and R. Gudgel,
527 2011: Statistical-dynamical predictions of seasonal North Atlantic hurricane activity.
528 *Mon. Wea. Rev.*, 139, 1070–1082.

529 Villarini, G., and G.A. Vecchi, 2012: Twenty-first-century projections of North Atlantic tropical
530 storms from CMIP5 models. *Nature Climate Change*, **2**, 604–607.
531 Walsh, K. J. E., and Coauthors, 2013: U.S. CLIVAR hurricane working group. *Bull. Amer.*
532 *Meteor. Soc.*, to be submitted.
533 Wang, H., A. Kumar, W. Wang, and B. Jha, 2012: U.S. summer precipitation and temperature
534 patterns following the peak phase of El Niño. *J. Climate*, **25,** 7204–7215.
535 Wang, H., Y. Pan, A. Kumar, and W. Wang, 2013: Modulation of convectively coupled Kelvin
536 wave activity in the tropical Pacific by ENSO. *Acta Meteor. Sinica*, **27,** 295–307.
537 Wang, H., J.-K. E. Schemm, A. Kumar, W. Wang, L. Long, M. Chelliah, G. D. Bell, and P.
538 Peng, 2009: A statistical forecast model for Atlantic seasonal hurricane activity based on
539 the NCEP dynamical seasonal forecast. *J. Climate*, **22,** 4481–4500.
540 Wilks, D. S., 1995: *Statistical Methods in the Atmospheric Sciences*. Academic Press, 467 pp.
541 Xie, P., and P. A. Arkin, 1997: Global precipitation: A 17-year monthly analysis based on gauge
542 observations, satellite estimates, and numerical model outputs. *Bull. Amer. Meteor. Soc.*,
543 **78,** 2539–2558.
544 Yeh, S.-W., J.-S. Kug, B. Dewitte, M.-H. Kwon, B. P. Kirtman, and F.-F. Jin, 2009: El Niño in a
545 changing climate. *Nature*, **461,** 511–514.
546 Zhao, M., and I. M. Held, 2010: An analysis of the effect of global warming on the intensity of
547 Atlantic hurricanes using a GCM with statistical refinement. *J. Climate*, **23,** 6382–6393.
548 Zhao, M., I. M. Held, S.-J. Lin, and G. A. Vecchi, 2009: Simulations of global hurricane
549 climatology, interannual variability, and response to global warming using a 50-km
550 resolution GCM. J. Climate, 22, 6653–6678.
551

552 **Figure Captions**

553 Fig. 1. Composites of ASO seasonal mean SST anomalies (unit: K) for (a) EP El Niño
554 (1982, 1986, 1991, 1997, and 2006), (b) CP El Niño (1987, 1994, 2002, 2004, and 2009), and (c)
555 La Niña (1983, 1984, 1988, 1995, 1998, 1999, 2005, and 2007) during 1982–2009. The
556 anomalies circled by light lines are above the 99% significance level estimated by the Monte
557 Carlo tests.

558 Fig. 2. Composites of TC track density (top row) and track density anomaly (middle row)
559 for (a),(d) EP El Niño, (b),(e) CP El Niño, and (c),(f) La Niña years, and distribution of TC
560 origins during (g) five EP El Niño, (h) five CP El Niño, and (i) five La Niña years derived from
561 observations. The anomalies circled by light lines (middle row) are above the 90% significance
562 level estimated by the Monte Carlo tests. The boxes with dash lines denote the main
563 development region (MDR; 10^{o}–20^{o}N, 20^{o}–80^{o}W).

564 Fig. 3. Time series of annual number of Atlantic TCs from 1982 to 2009 for observations
565 (OBS) and multi-model ensemble (MME) mean (thick lines with open circles), as well as
566 individual model ensemble means (thin lines). Grey shading denotes the range of ± one standard
567 deviation of the spreads of the five individual model ensemble means around the MME mean.

568 Fig. 4. Climatology of track density for (a) observations, (c)–(g) individual model
569 ensemble means, and (h) MME mean, and 28-yr total TC origins for (b) observations, (i)–(m)
570 one ensemble member of each model, and (n) MME total from one member of each model. The
571 boxes with dash lines denote the MDR.

572 Fig. 5. Composites of track density during EP El Niño (left column), CP El Niño (middle
573 column), and La Niña (right column) for five individual model ensemble mean (top five rows)
574 and MME mean (bottom row). The boxes with dash lines denote the MDR.

575 Fig. 6. Composites of track density anomaly during EP El Niño (left column), CP El Niño
576 (middle column), and La Niña (right column) for five individual model ensemble mean (top five
577 rows) and MME mean (bottom row). The anomalies circled by light lines are above the 90%
578 significance level estimated. The boxes with dash lines denote the MDR.

579 Fig. 7. Distribution of TC origins during five EP El Niño (left column), five CP El Niño
580 (middle column), and five La Niña (right column) years from one ensemble member of each
581 model (top five rows) and MME total from one member of each model (bottom row). The boxes
582 with dash lines denote the MDR.

583 Fig. 8. (a) Observed ASO season climatology of vertical shear of zonal wind (unit: m s^{-1})
584 between 200 and 850 hPa and mean bias in the (b) FSU, (c) GFDL, (d) GISS, (e) GSFC, and (f)
585 GFS models, as well as (g) the MME. The boxes with dash lines denote the MDR.

586 Fig. 9. Composites of ASO seasonal mean vertical wind shear anomalies (unit: m s^{-1}) for
587 (a),(d) EP El Niño, (b),(e) CP El Niño, and (c),(f) La Niña during 1982–2009 in observations
588 (top row) and the MME mean (bottom row). The anomalies circled by light lines are above the
589 90% significance level. The boxes with dash lines denote the MDR.

590 Fig. 10. Composites of ASO seasonal mean precipitation anomalies (unit: mm day^{-1}) for
591 (a),(d) EP El Niño, (b),(e) CP El Niño, and (c),(f) La Niña during 1982–2009 in observations
592 (left column) and the MME mean (right column). The anomalies circled by light lines are above
593 the 99% significance level.

594 Fig. 11. Changes in vertical wind shear (unit: m s^{-1} K^{-1}) associated with a westward shift
595 of warm SST anomalies from the Niño-3 region (5^oS – 5^oN, 90^o – 150^oW) to the Niño-4 region
596 (5^oS – 5^oN, 150^oW – 160^oE). The boxes with solid lines denote the MDR.
597

598 Table 1. List of five GCMs for the HWG interannual experiments, the number of
599 ensemble members, model data grid, and references for TC tracking algorithms.
600

Model	Ensemble members	Model data grid zonal×meridional	Tracking algorithm
FSU	3	384 × 192	LaRow et al. (2008)
GFDL	3	576 × 360	Zhao et al. (2009)
NASA GISS	3	360 × 180	Camargo and Zebiak (2002)
NASA GSFC	2	576 × 361	LaRow et al. (2008)
NCEP GFS	5	360 × 181	Camargo and Zebiak (2002)

601

602

603 Table 2. List of TC statistics for observations (OBS), multiple model ensemble (MME)
604 mean, and individual model ensemble means, including 28-yr (1982–2009) long-term mean
605 annual number of Atlantic TCs, variance of interannual variability, linear trend (increase of TCs
606 per decade), anomaly correlation (AC) between observations and model simulated interannual
607 TC anomalies, and root-mean-square error (RMSE). The variance for each model is the average
608 of the variance derived from individual ensemble members.
609

Model	Mean	Variance	Trend	AC	RMSE
OBS	11.7	25.9	3.7		
MME	13.1	17.0	1.9	0.86	3.5
FSU	13.5	9.2	1.7	0.62	4.5
GFDL	12.7	16.4	2.2	0.74	3.6
GISS	6.2	8.8	1.1	0.68	6.7
GSFC	10.9	24.5	2.6	0.62	4.2
GFS	22.0	26.1	2.1	0.73	10.9

610

611

612 Table 3. Mean annual number of TCs over the entire 28 years, five EP El Niño, five CP
613 El Niño, and eight La Niña years, respectively, for observations (OBS), MME, and individual
614 model ensemble means. Values in parentheses are the percentages of the 28-yr climatology.

615

Model	Mean	EP El Niño	CP El Niño	La Niña
OBS	11.7	6.8 (58%)	10.2 (87%)	14.6 (125%)
MME	13.1	10.4 (80%)	12.4 (95%)	14.5 (111%)
FSU	13.5	11.9 (88%)	12.0 (89%)	15.3 (113%)
GFDL	12.7	9.5 (75%)	11.0 (87%)	15.5 (122%)
GISS	6.2	4.5 (73%)	5.7 (91%)	7.3 (117%)
GSFC	10.9	6.9 (63%)	12.9 (118%)	11.2 (102%)
GFS	22.0	19.3 (88%)	20.5 (93%)	23.1 (105%)

616

617

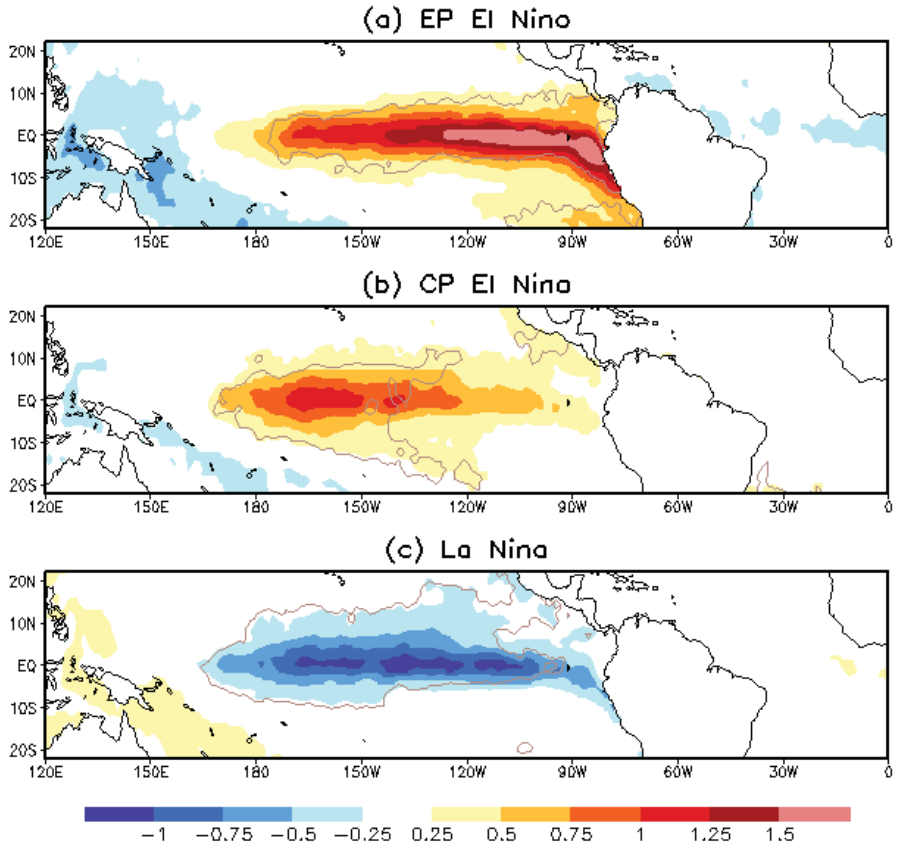

Fig. 1. Composites of ASO seasonal mean SST anomalies (unit: K) for (a) EP El Niño (1982, 1986, 1991, 1997, and 2006), (b) CP El Niño (1987, 1994, 2002, 2004, and 2009), and (c) La Niña (1983, 1984, 1988, 1995, 1998, 1999, 2005, and 2007) during 1982–2009. The anomalies circled by light lines are above the 99% significance level estimated by the Monte Carlo tests.

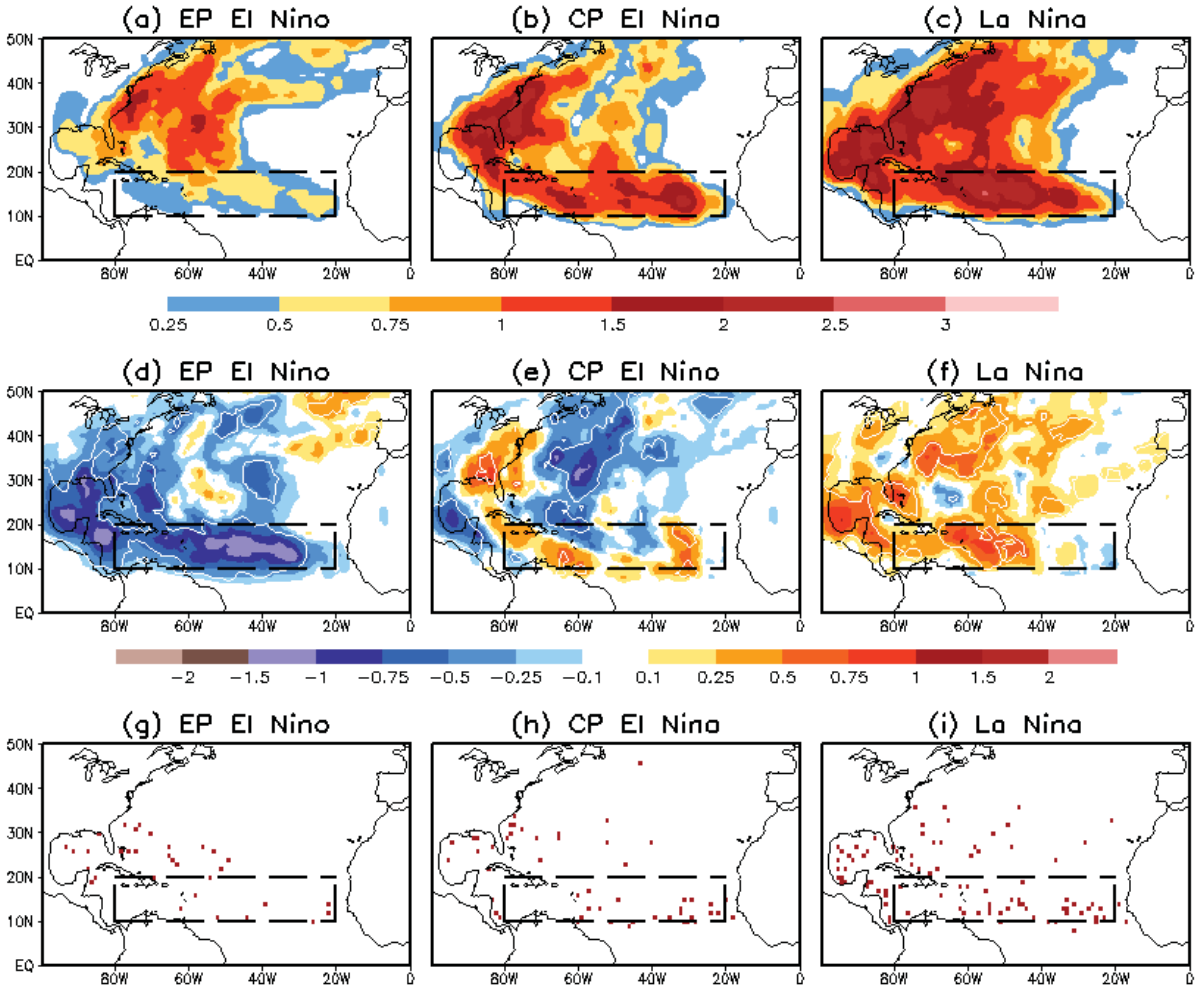

Fig. 2. Composites of TC track density (top row) and track density anomaly (middle row) for (a),(d) EP El Niño, (b),(e) CP El Niño, and (c),(f) La Niña years, and distribution of TC origins during (g) five EP El Niño, (h) five CP El Niño, and (i) five La Niña years derived from observations. The anomalies circled by light lines (middle row) are above the 90% significance level estimated by the Monte Carlo tests. The boxes with dash lines denote the main development region (MDR; 10°–20°N, 20°–80°W).

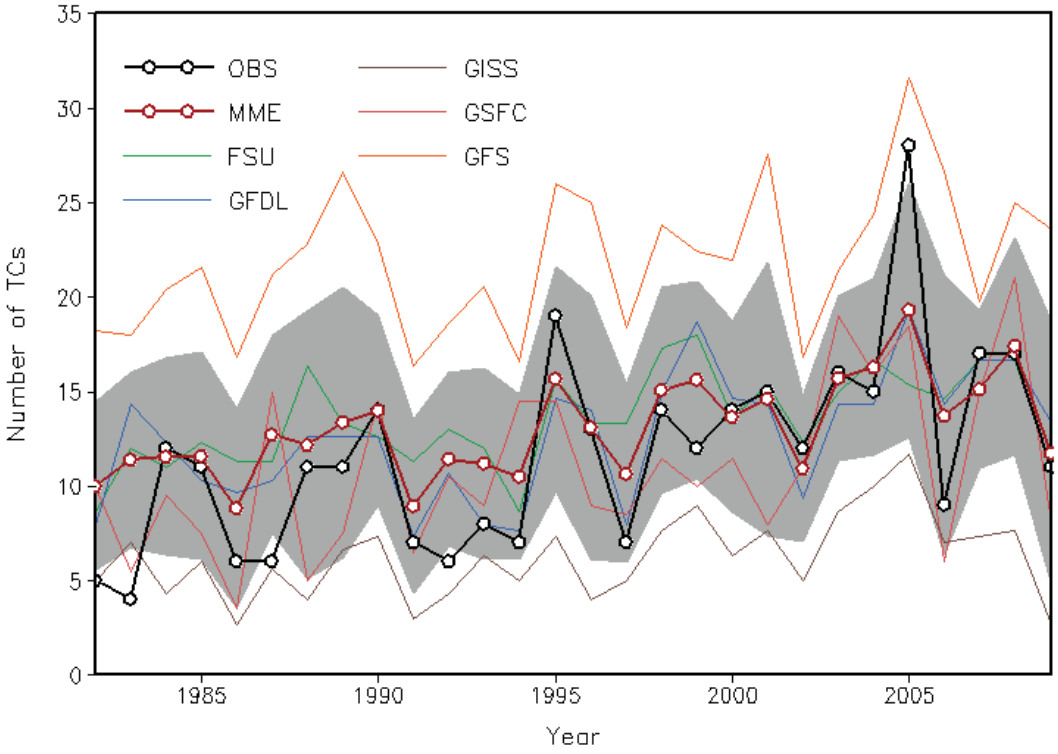

Fig. 3. Time series of annual number of Atlantic TCs from 1982 to 2009 for observations (OBS) and multi-model ensemble (MME) mean (thick lines with open circles), as well as individual model ensemble means (thin lines). Grey shading denotes the range of ± one standard deviation of the spreads of the five individual model ensemble means around the MME mean.

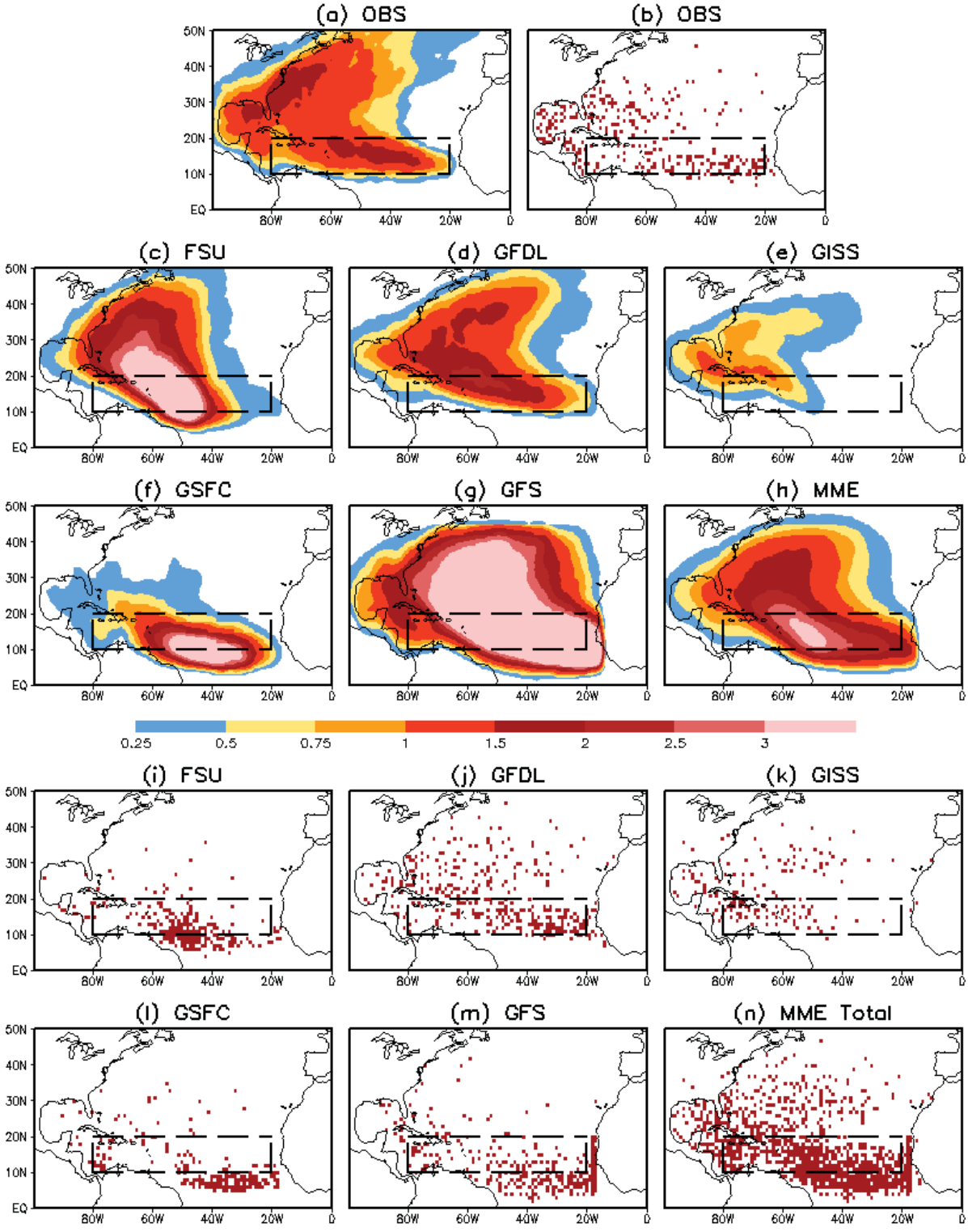

Fig. 4. Climatology of track density for (a) observations, (c)–(g) individual model ensemble means, and (h) MME mean, and 28-yr total TC origins for (b) observations, (i)–(m) one ensemble member of each model, and (n) MME total from one member of each model. The boxes with dash lines denote the MDR.

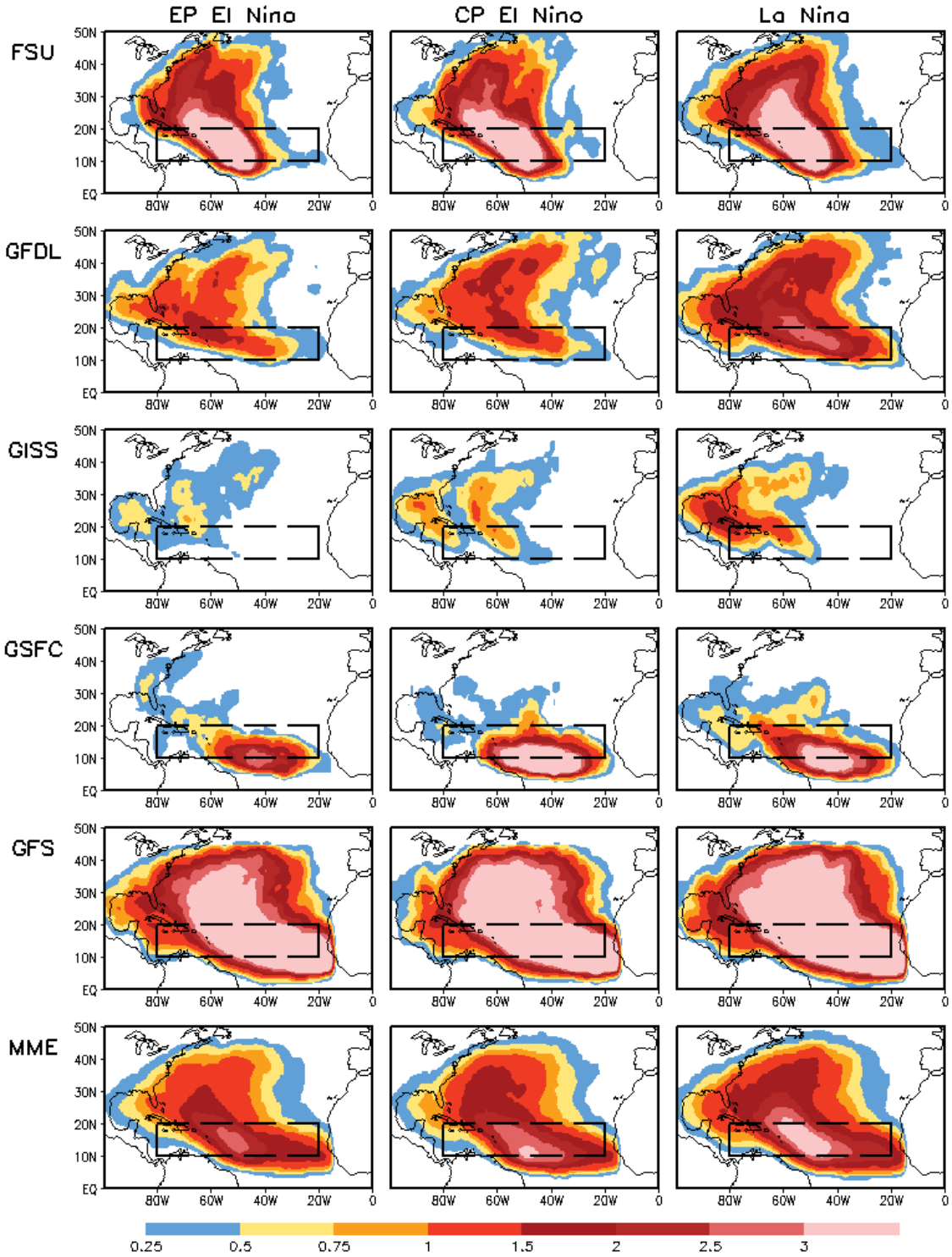

Fig. 5. Composites of track density during EP El Niño (left column), CP El Niño (middle column), and La Niña (right column) for five individual model ensemble mean (top five rows) and MME mean (bottom row). The boxes with dash lines denote the MDR.

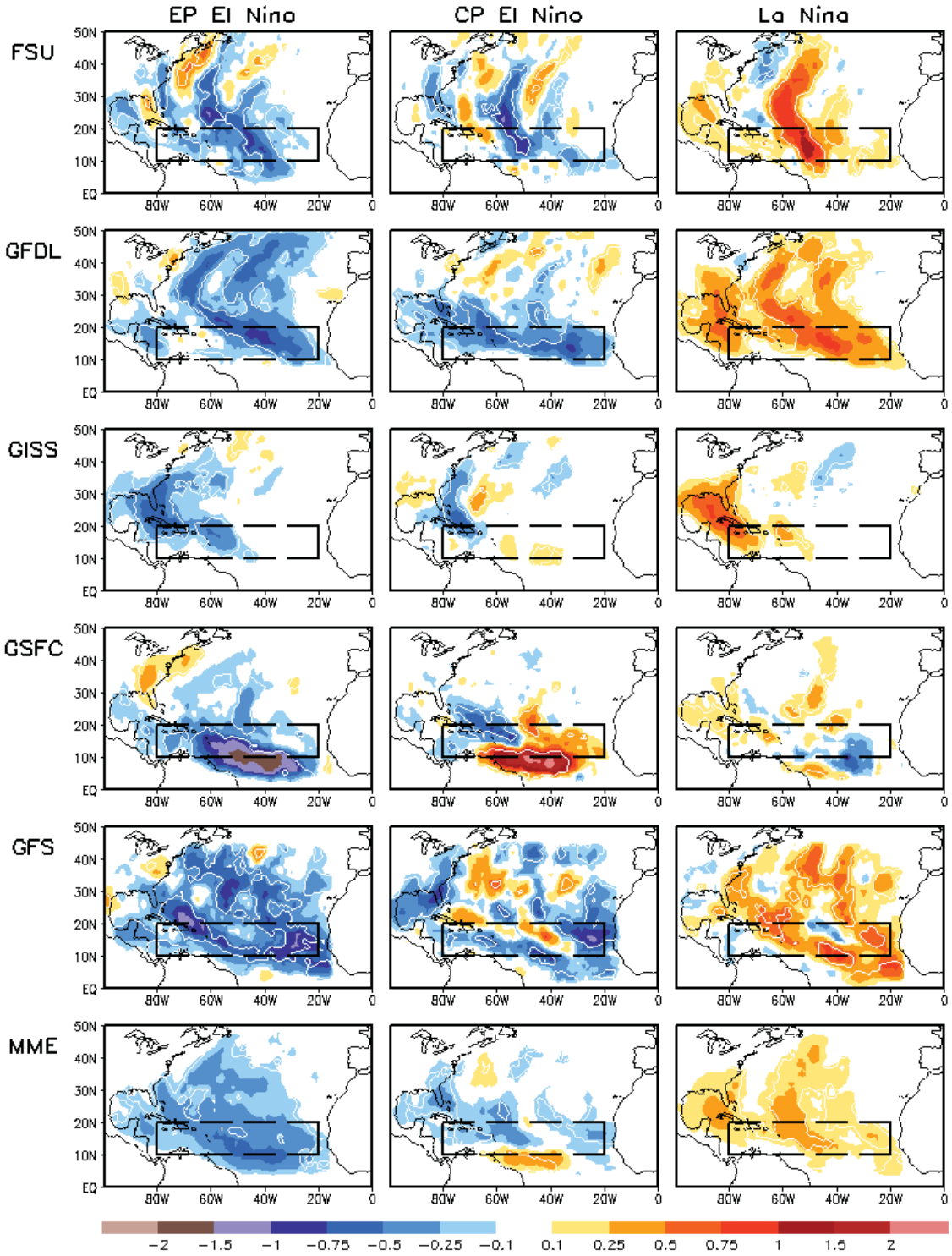

Fig. 6. Composites of track density anomaly during EP El Niño (left column), CP El Niño (middle column), and La Niña (right column) for five individual model ensemble mean (top five rows) and MME mean (bottom row). The anomalies circled by light lines are above the 90% significance level estimated. The boxes with dash lines denote the MDR.

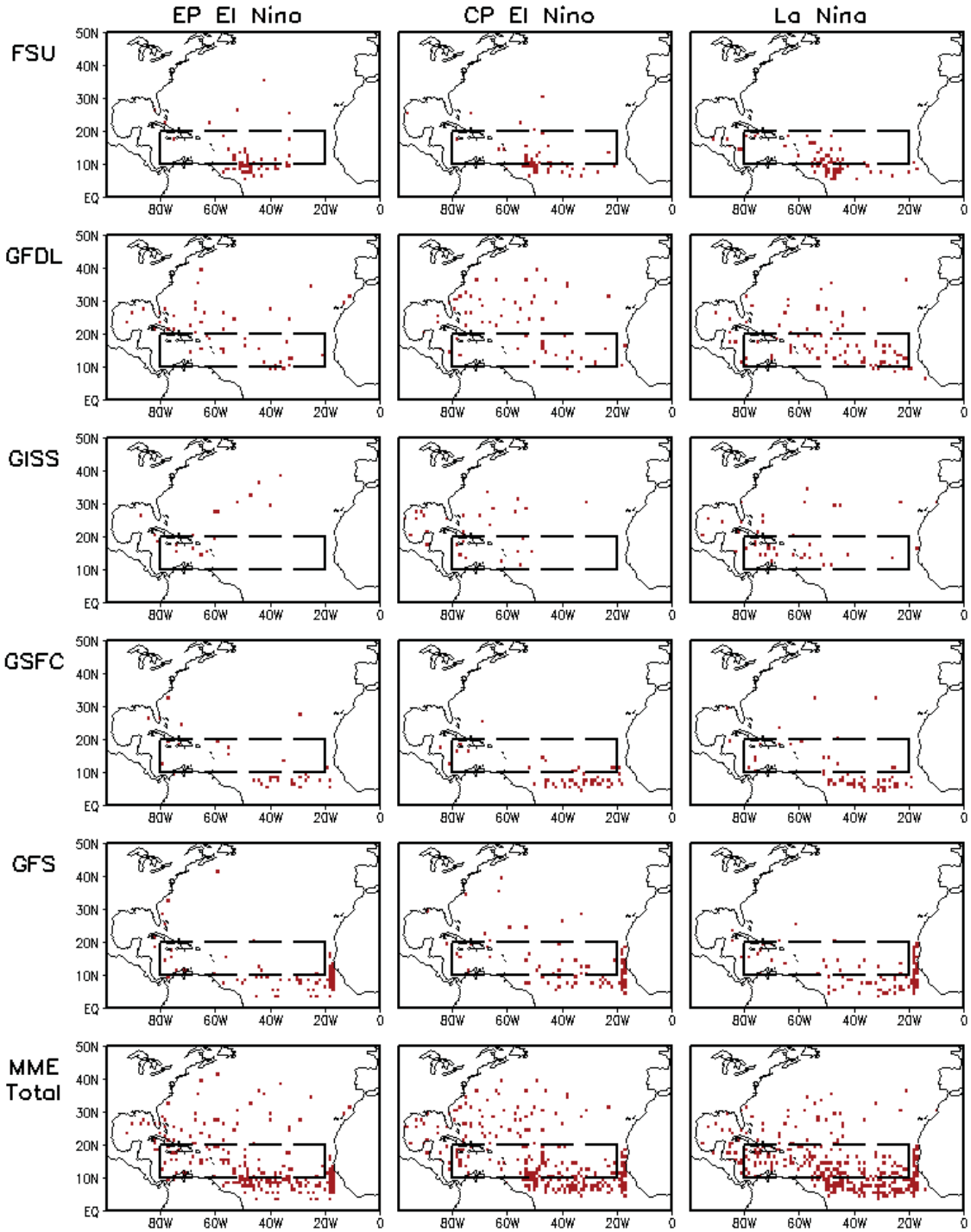

Fig. 7. Distribution of TC origins during five EP El Niño (left column), five CP El Niño (middle column), and five La Niña (right column) years from one ensemble member of each model (top five rows) and MME total from one member of each model (bottom row). The boxes with dash lines denote the MDR.

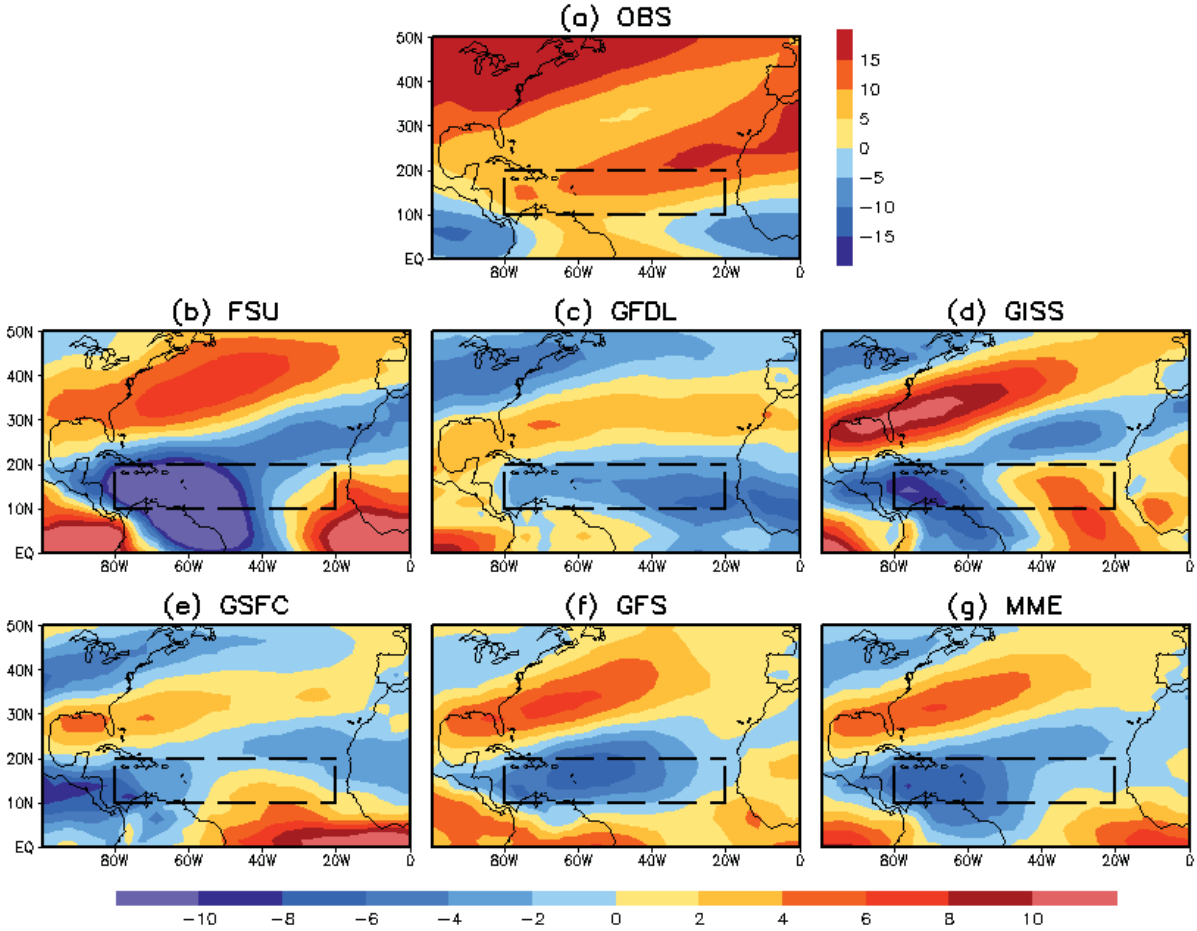

Fig. 8. (a) Observed ASO season climatology of vertical shear of zonal wind (unit: m s^{-1}) between 200 and 850 hPa and mean bias in the (b) FSU, (c) GFDL, (d) GISS, (e) GSFC, and (f) GFS models, as well as (g) the MME. The boxes with dash lines denote the MDR.

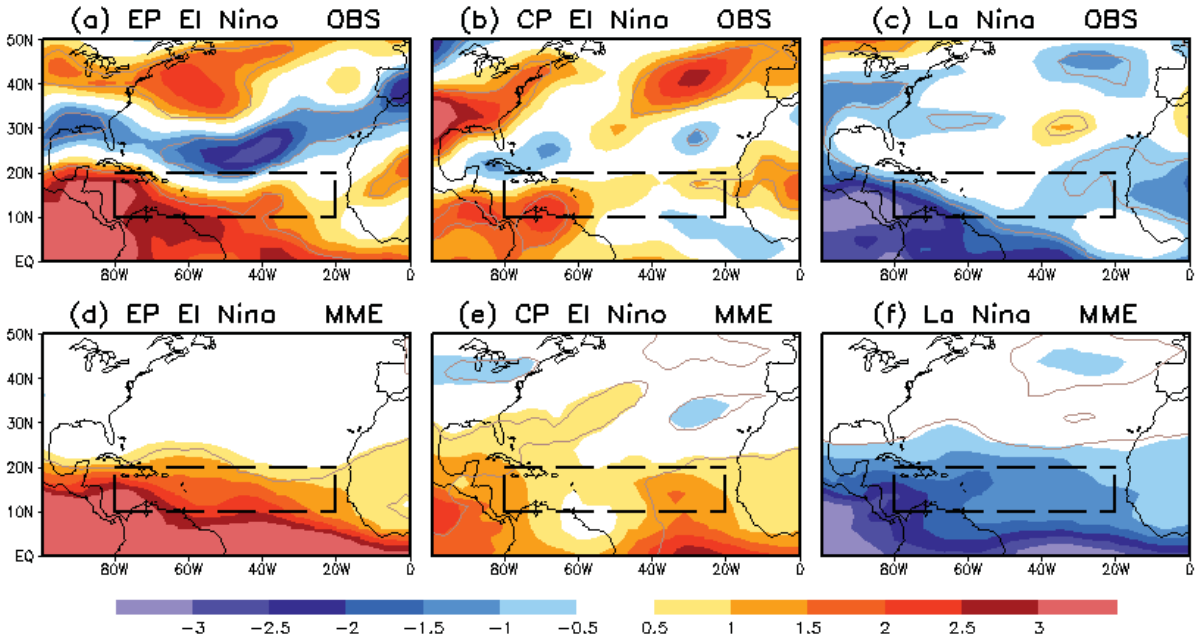

668
669 Fig. 9. Composites of ASO seasonal mean vertical wind shear anomalies (unit: m s^{-1}) for
670 (a),(d) EP El Niño, (b),(e) CP El Niño, and (c),(f) La Niña during 1982–2009 in observations
671 (top row) and the MME mean (bottom row). The anomalies circled by light lines are above the
672 90% significance level. The boxes with dash lines denote the MDR.
673

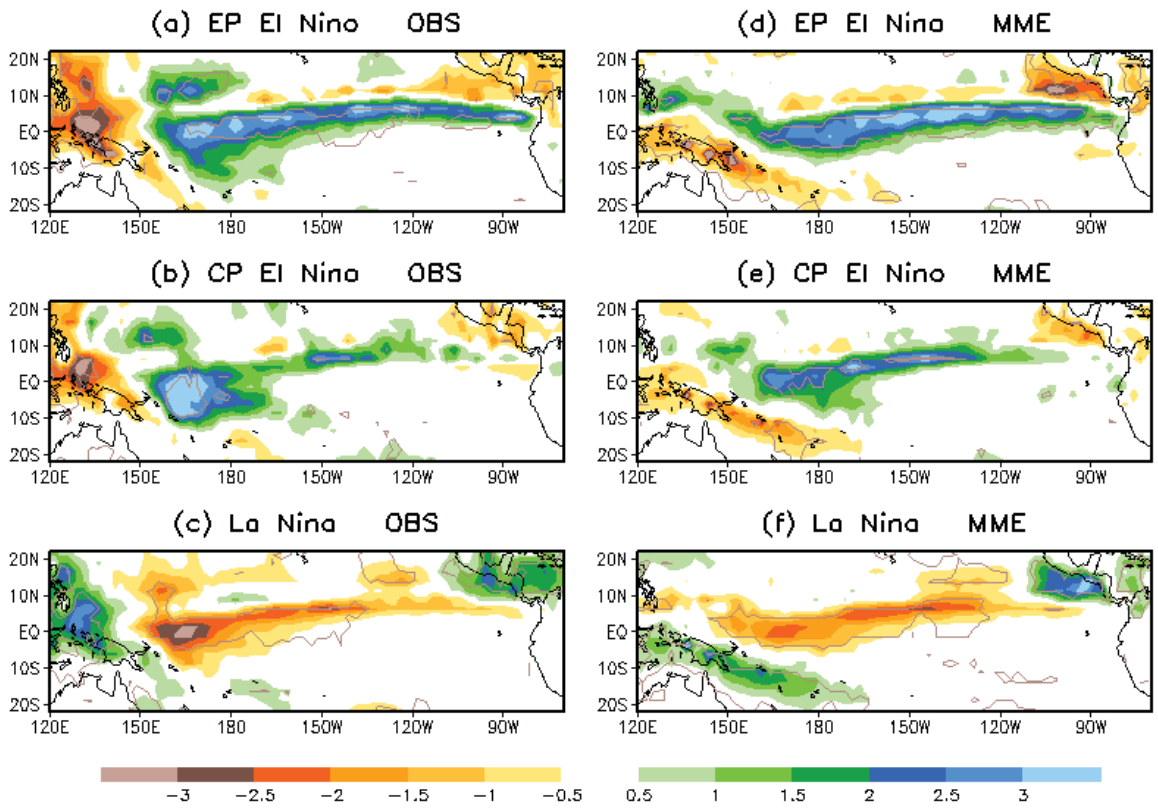

674
675 Fig. 10. Composites of ASO seasonal mean precipitation anomalies (unit: mm day^{-1}) for
676 (a),(d) EP El Niño, (b),(e) CP El Niño, and (c),(f) La Niña during 1982–2009 in observations
677 (left column) and the MME mean (right column). The anomalies circled by light lines are above
678 the 99% significance level.
679

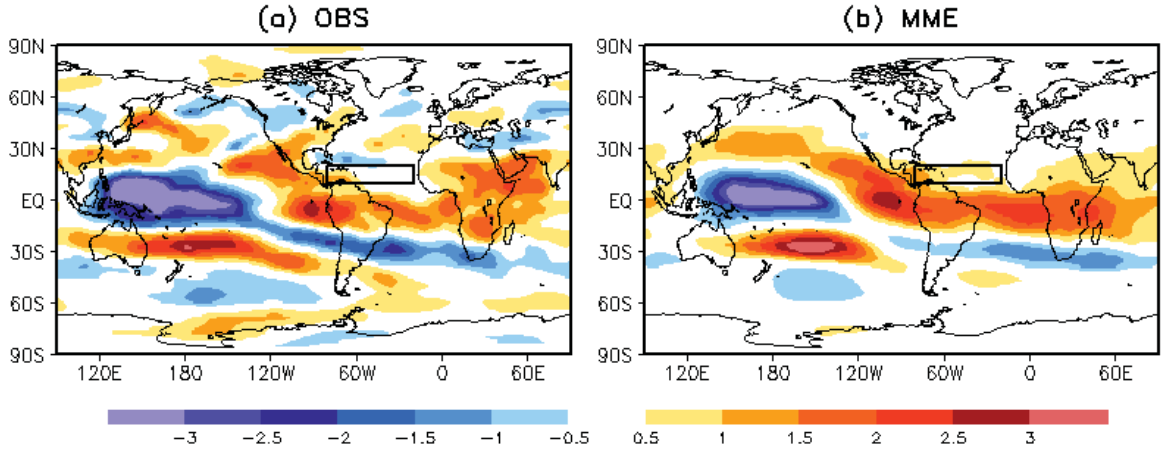

Fig. 11. Changes in vertical wind shear (unit: m s^{-1} K^{-1}) associated with a westward shift of warm SST anomalies from the Niño-3 region (5°S – 5°N, 90° – 150°W) to the Niño-4 region (5°S – 5°N, 150°W – 160°E). The boxes with solid lines denote the MDR.